Structural reordering and electrical activation of ion-implanted GaAs and InP due to laser annealing in a controlled atmosphere

G. Vitali, C. Pizzuto, and G. Zollo
Dipartimento di Energetica, Università La Sapienza and INFM, Via A. Scarpa 14, 00161 Rome, Italy

D. Karpuzov
Institute of Electronics, Bulgarian Academy of Sciences, Boulevard Tzarigradsko Chaussee 72, Sofia 1784, Bulgaria

M. Kalitzova
Institute of Solid State Physics, Bulgarian Academy of Sciences, Boulevard Tzarigradsko Chaussee 72, Sofia 1784, Bulgaria

P. van der Heide
Surface Science Western, The University of Western Ontario, London, Ontario, Canada N6A 587

G. Scamarcio, V. Spagnolo, and L. Chiavarone
Dipartimento Interateneo di Fisica di Bari and INFM, Via Amendola 173, 70126 Bari, Italy

D. Manno
Dipartimento di Scienza dei Materiali, Università di Lecce and INFM, via per Arnesano, 73100 Lecce, Italy
(Received 29 July 1998)

The effects of the ambient atmosphere in the annealing chamber on the electrical and structural characteristics of Zn-implanted III-V compound semiconductors, processed by low-power pulsed-laser annealing are presented. The samples were analyzed using several complementary experimental techniques: Reflection high-energy electron diffraction, Rutherford backscattering spectroscopy, Raman spectroscopy, secondary ion mass spectroscopy, and electrical measurements. During the laser beam irradiation in the presence of gas inlet into the annealing chamber the ambient gas atoms diffused well into the target changing the stoichiometry and the electrical parameters. Redistribution of the implanted impurity was also observed. By varying the type of gas used and its pressure, it was possible to achieve electrical activation of up to 80%. It seems all structure and electrical parameters achieve their best values at the same ambient atmosphere and density of the deposited laser power P, e.g., 1.5 atm of N_2 and $P = 6.5$ MW/cm^2 for InP. [S0163-1829(99)12803-0]

I. INTRODUCTION

In recent years, remarkable interest has been paid to the advantages of using compound semiconductors such as GaAs and InP in optoelectronic and microwave device technology. Among these materials, InP seems to be particularly attractive (e.g., for fiber optics applications) due to higher values of the peak electron drift velocity and the breakdown field with respect to other similar materials such as GaAs and Si.[1–8] In addition, the combination of high-radiation resistance and electrical efficiency makes InP very attractive for solar cells manufacturing in aerospace technology.[9,10] Finally, indium phosphide is promising substrate material for the fabrication of field-effect transistors, avalanche photodiodes and IMPATT diodes.[11] Most recently, particular interest was paid to the study of nitride-related compounds due to their potential application in short-wavelength optical devices such as blue light-emitting diodes.[12–16] The nitrides on InP are also attractive for surface passivation of special devices.[17]

The electrical properties of implanted InP have been studied in several papers.[18–25] The results reported in the literature show that a high-peak carrier concentration of 10^{19} cm^{-3} is achievable in substrated doped with n-type implants. the p-type dopants in InP are known to have lower activation efficiency. In this case a maximum sheet hole concentration of 10^{13} cm^{-2} and an electrical activation below 50% have been obtained instead. The values correlate with the broadening of the implant profile observed, due to inward diffusion of p-type dopants during the subsequent elevated temperature annealing,[18–22] required to recover the high-density damage.

We recently reported data on application of low-power pulsed-laser annealing (LPPLA) technique to ion-implanted GaAs and InP.[26] The LPPLA was carried directly in air to make it work in the cheapest and easiest way, but the formation of laser-induced surface oxide was demonstrated to play a crucial role. This layer was particularly restrictive in the case of InP material, since it reduced the efficiency of using repetitive laser pulses. It was concluded that LPPLA processing in vacuum is not good enough and a controlled ambient of Ar or N_2 is needed to prevent formation of surface oxides.

The purpose of the present paper is to provide and compare results obtained by applying the LPPLA processing to GaAs and InP samples in vacuum and in a controlled atmosphere. The following complementary analytical techniques were used in the investigations: high resolution cross-section transmission electron microscopy (HRXTEM), reflection

 ©1999 The American Physical Society

high-energy electron diffraction (RHEED), Rutherford backscattering spectroscopy (RBS), secondary ion mass spectroscopy (SIMS), microRaman spectroscopy (MRS), and electrical measurements.

In order to facilitate the interpretation of the obtained results it is worth summarizing the main mechanisms involved in the solid-phase epitaxy induced by LPPLA, according to Ref. 26. The most essential experimental condition to achieve good-quality laser annealing is that the sample temperature must be kept far below the melting value at any point of the surface. Furthermore, in compound semiconductors it should be below the stoichiometric decomposition temperature, too. In these conditions, the invoked process of crystalline solid-state regrowth is probably connected with destabilization of the lattice, which occurs when a critical density of valence-band electrons is photoexcited after absorbing the laser radiation.

When the damage induced by ion implantation is not homogeneous, which is common at implantation doses below $1\text{-}5\times10^{14}$ ions cm^{-2},[27] local thermal gradients and subsequent mechanical stresses rise up. They facilitate the drifting of mainly unstable interstitial point defects through the destabilized lattice and their recombination with vacancies. The duration of these processes is of the order of 10^{-11} s (jumping time[28]). Since the laser pulse duration is about 10^{-8} s, it is reasonable to expect that several jumpings occur during the laser treatment, normally consisting of a sequence of 20 laser pulses, about.

II. EXPERIMENT

A. Materials and processing

The specimens used consisted of semi-insulating GaAs and InP (100) single-crystal wafers (Sumitomo Corporation Ltd., Japan) 400-μm thick. They were implanted with 140-keV Zn^+ ions to a dose of 10^{14} cm^{-2} at 7° from the sample normal. The ion current did not exceed 2 μA cm^{-2}, and the samples were intentionally heated during the implantation processing to keep the temperature at 110 ± 10 °C.

To avoid the surface micromelting, appearing at 9 MW/cm^2 for GaAs and 11 MW/cm^2 for InP, respectively, the implanted samples were irradiated with 20 consecutive ruby-laser pulses of $\Delta t_{\mathrm{FWHM}}=25$ ns with a frequency of 0.05 Hz. The average power density of the pulses used in the processing (in the range of 5.5 to 7 MW/cm^2) was expected to result in effective lattice recovery.[29]

B. Electron microscope observations

The crystal structure of the GaAs and InP samples, both before and after the annealing, was controlled in a AEI EM6G Electron Microscope. It was equipped with a high-resolution electron-diffraction stage, which allows the sample rotation around the normal to the surface and, as a consequence, the observation of reflection-diffraction patterns corresponding to different azimuth directions.

The cross-sectional specimens were obtained by preparing sandwich structures of (011) cut slices from (100) GaAs substrates only. The sandwiches were mechanically prethinned, dimpled, and, as a last step, etched by Ar^+ beam at RT until the electron transparency occurred. The HRTEM observations were carried out in a JEM 2010 electron microscope operating at an acceleration voltage of 160 kV.

C. RBS analysis

The samples were analyzed by using 1.5 MeV accelerated He^+ beam, incident normally onto the specimen surface. Spectra in both random and channeled mode were collected at a scattering angle of 160°. The detector sensitivity was 3.153 keV/ch and the collected current was about 4 μA. The recorded spectra for samples before and after the laser treatment were processed to extract the polynomial fit to the background of the surface damage peak and to obtain the depth distribution of defects induced by the treatment itself.

D. SIMS measurements

SIMS depth profiling was carried out on a Cameca IMS-3f instrument. The primary ion beam consisted of a 50 nA Cs^+ with an incident energy of 2 keV rastered over a 250×250 μm^2. The contrast aperture, field aperture and image field were set at 400, 750, and 150 μm, respectively.

The Cs^+, NCs^+, and $ZnCs^+$ ions were measured since this allows for improved depth resolution, increases sensitivity (especially in the case of N) and a reduction of any matrix effect present. Concentration versus depth plots were derived for Zn by normalizing the area under the $ZnCs^+$. Cs^+ versus depth curves to the known implanted dose. Depth scales were defined using DekTak IIA surface profilometer.

E. Micro-Raman spectroscopy

Micro-Raman spectroscopy measurements were performed at RT using a Jobin Yvon T64000 triple spectrometer equipped with a N_2 cooled CCD detection system. The slits were set at resolution of 0.6 cm^{-1}. The spectra were recorded in backscattering geometry from the sample surface, using the 5145- and 4579-Å lines of an Ar^+ laser.

F. Electrical measurements

The sheet resistivity measurements were carried out by using the Van der Pauw (VdP) method. In our case the current source and the voltage meter were integrated in a single instrument (Keitley 236). The commutations between the typical configurations of the VdP method were realized using a manual commutator. The Hall measurements have been performed by using a 2T Bruker magnetic-field generator.

III. RESULTS AND DISCUSSION

As already pointed out briefly in the Introduction, LPPLA experiments require that the temperature of the irradiated sample does not exceed a critical value T_c above which the alteration of the stoichiometric ratio becomes substantial. It was shown, that as a consequence, the LPPLA is efficient within a well-defined range of the laser power density only. Following the model and the calculations already reported in Ref. 26, the irradiation power densities used in this work were set at 5.5 MW/cm^2 for GaAs (that results in a tempera-

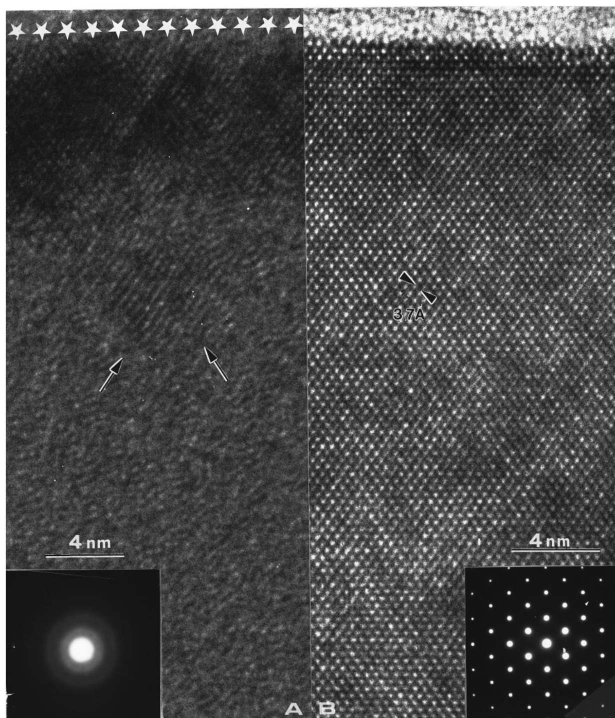

FIG. 1. XHRTEM micrographs, ⟨110⟩ projection of 140 keV Zn-implanted (100) GaAs. The inserts show the corresponding selected area diffraction patterns: (a) As-implanted surface layer. Arrows show crystal islands buried in the amorphized layer after the implantation. (b) LPPLA restored crystal lattice of the same layer.

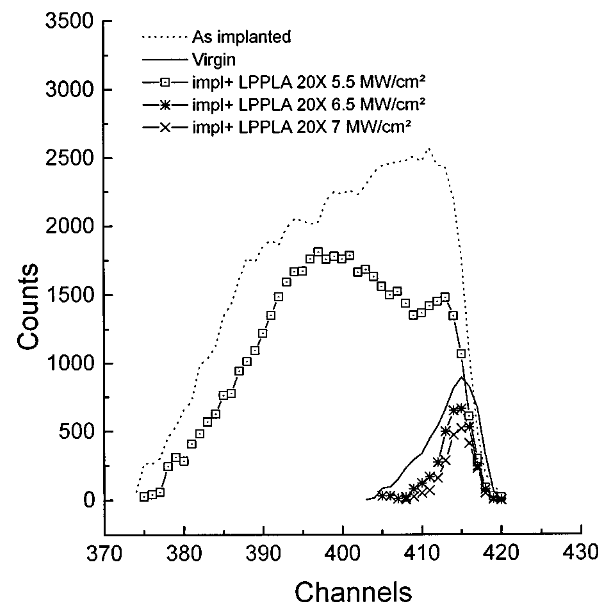

FIG. 2. RBS spectra in channeling mode. The peak corresponding to the surface damage is shown for virgin, as-implanted, and implanted plus LPPLA treated specimens of InP.

ture increase of the irradiated surface to about 580 °C), and 6.5 MW/cm^2 for InP (yielding a temperature rise to nearly 290 °C). In any case the RHEED analyses did not reveal any substantial structure changes for laser treatment at densities below 5.0 MW/cm^2 for both GaAs and InP.[26]

LPPLA experiments were carried out in vacuum (10^{-7} atm) and in Ar or N_2 ambient at pressures of 0.5, 1, 1.5, and 2 atm. The influence of the annealing atmosphere on the electrical activation of the implanted ions is followed by comparing the results for various samples obtained by electrical measurements and using complementary techniques outlined above.

A. XHRTEM analysis of structure reordering

In Fig. 1, one can find illustrated the (110) lattice plane imaging projections of cross-sectioned specimens of GaAs. The maximum of the ion-beam-induced radiation damage [Fig. 1(a)] appears as a continuous amorphouslike structure, see the diffraction pattern in the insert. It is located between approximately 20 and 50 nm below the implanted surface, as shown by the stars in Fig. 1(a). The residual crystalline zones, clearly visible in Fig. 1(a), play a crucial role in the epitaxial regrowth induced by LPPLA.[27] One can note that some of these zones extend from the residual surface crystalline region toward the amorphized layer. Others appear as rather small crystalline islands embedded in this layer. These regions probably originate from local zones where the ion-beam-deposited energy density is lower than the critical value required for the transition to amorphous phase.

After the laser irradiation, carried out with 20 consecutive pulses of 5.5 MW/ cm^2 each, the crystal order of GaAs appears almost completely restored, as seen in Fig. 1(b). The selected area diffraction pattern shown in the insert comes from a circular area of about 100 nm in diameter and confirms the efficiency of the LPPLA processing.

B. RBS analysis of the structural damage

The RBS spectra of InP samples in channeling mode are illustrated in Fig. 2. The In-component surface peak is shown for (i) virgin, (ii) as-implanted and (iii) implanted and then annealed wafers. The samples were annealed in N_2 ambient at a pressure of 1 atm, with different laser power densities as indicated in the figure. The background of each spectrum is subtracted according to the ''surface approximation'' approach. As expected, the spectrum of the as-implanted sample gives the highest yield resulting from the ion-beam-induced structural disorder. The damage yields of the annealed samples are lower than that of the as-implanted one, for all depths studied being even lower than the yield of the virgin sample if the irradiated power density is $\geqslant 6.5$ MW/cm^2. This behavior supports the idea that the LPPLA treatment with suitable power density of the laser pulse can remove even the shallow surface disorder caused by final polishing procedures of the wafer manufacturing. It is worth noting here that studies of the composition impose a limit on the LPPLA power density for treatment of InP samples up to 6.5 MW/cm^2, to avoid surface stoichiometric alteration of the compound at higher irradiation power densities.

C. SIMS analysis

In Fig. 3 the SIMS depth versus concentration profiles of Zn are shown for as-implanted and annealed InP samples at different irradiation power densities. The annealing was completed keeping the samples in N_2 ambient at 1.5 atm. The maximum position of the as-implanted Zn profile agrees well with that obtained by simulation, using TRIM95 computer code ($Rp = 74.3$ nm). The experimentally measured

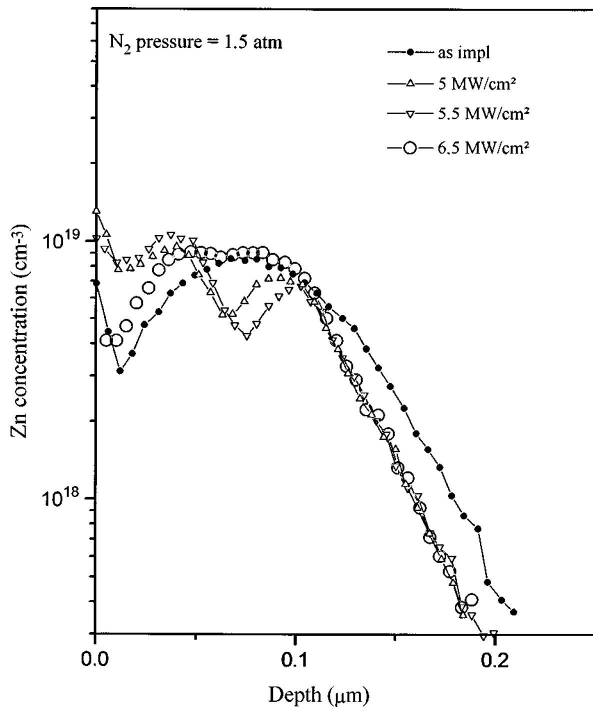

FIG. 3. SIMS depth profiles of Zn concentration in as-implanted and implanted plus laser annealed InP samples. The LPPLA processing was carried out by 20 pulses at different power densities, the ambient in the annealing chamber being nitrogen at pressure of 1.5 atm.

straggling $\Delta Rp_{\mathrm{exp}} \approx 55$ nm is larger than that of the calculated value 32 nm. The deviation is probably related to the elevated temperature during the implantation and the atomic relocation (mixing) during the analysis.

Zn distributions obtained after processing by LPPLA in two different ambient conditions in the annealing chamber: vacuum (6×10^{-8} atm) and N_2 at 1.5 atm are compared in Fig. 4. As one can see, only in the latter case we find a flat distribution with nearly constant zinc concentration in a wide interval of depths. On the contrary, in the case of LPPLA in vacuum (6×10^{-8} atm), the surface Zn concentration greatly rises probably due to the decrease of Zn sublimation temperature in vacuum. Moreover, some tendency of Zn diffusion toward the surface results to be present also in samples annealed in N_2 atmosphere.

It appears clearly from the reported spectra that the laser treatment induces Zn redistribution depending on the irradiation power density. In particular we obtained a flat Zn distribution extending from 30 to 100 nm in the sample treated with 6.5 MW/cm^2. There are several driving forces behind this displacement process, including the concentration gradients of the implanted zinc and of the bombardment-induced vacancy distributions, in addition to temperature gradients due to the adsorbed laser power. High-density photoexcitation of bonding electrons causes structure instability and atomic rearrangement within a few hundred femtoseconds.[30] Laser energy is transferred to the lattice in several picoseconds, generating thermal and mechanical stresses that affect the point defects. The effect is depending on the laser power density, and most prominently, on the distribution of temperature gradients in the substrate. In Fig. 5, the distribution of the space temperature gradient in Zn-implanted sample of

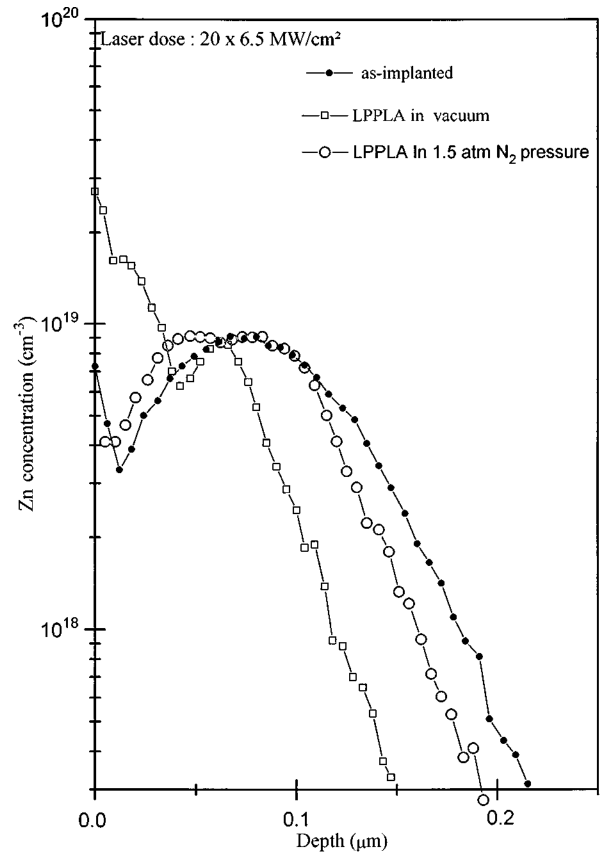

FIG. 4. SIMS depth profiles of Zn concentration in as-implanted and implanted plus laser-annealed samples of InP. Integral laser dose is $D=20\times 6.5$ MW/cm^2, LPPLA treatment was in vacuum or N_2 ambient.

InP, following the exposure to a laser pulse of 6.5 MW/cm^2, vs time and depth are shown. The lighter and darker zones correspond respectively to higher and lower absolute values of the gradient.[26] The plot indicates the existence of regions

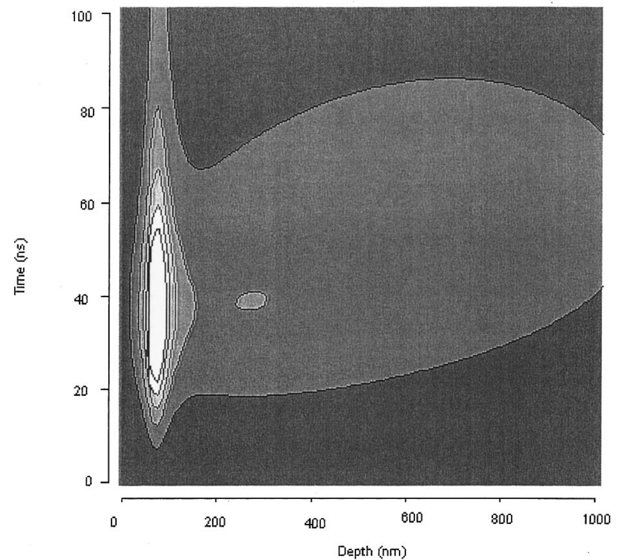

FIG. 5. Contour plot of the temperature space-gradient distribution (K cm^{-1}) vs time and depth for Zn-implanted InP sample, following a laser pulse of 6.5 MW/cm^2. Lighter zones indicate time-space region where this gradient is higher.

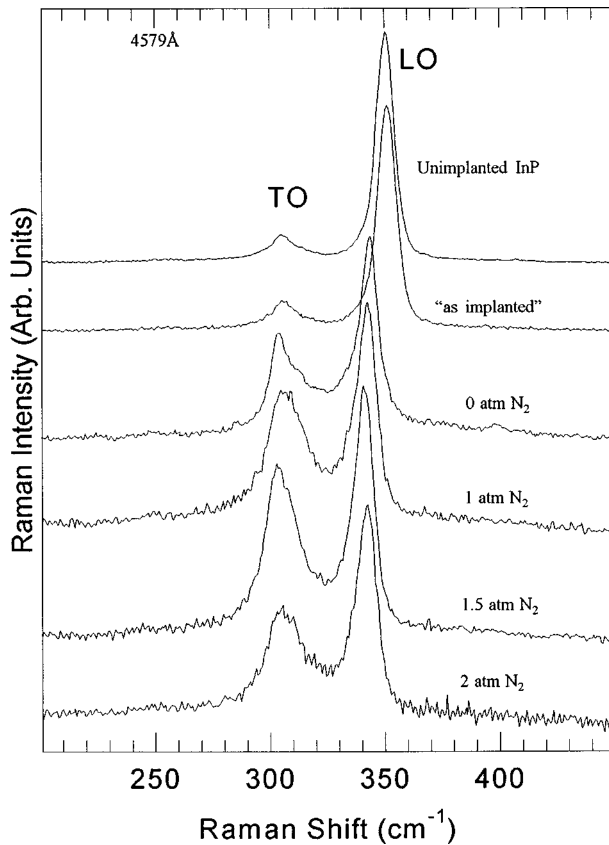

FIG. 6. Raman spectra, excited from Zn-implanted InP surface in backscattering configuration with laser pulse at 4579 Å wavelength. The N_2 pressure in the annealing chamber is indicated. The peaks LO and TO correspond to the longitudinal and transverse optical phonons in InP.

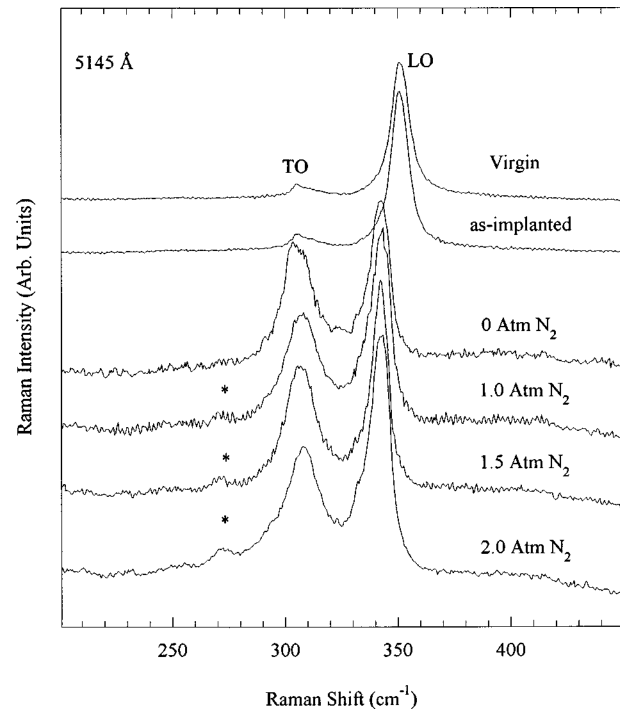

FIG. 7. Raman spectra, excited from Zn-implanted InP surface in backscattering configuration with laser wavelength of 5145 Å. The N_2 pressure in the annealing chamber is indicated. The peaks LO and TO correspond to the longitudinal and transverse optical phonons in InP. Labeled with stars are the additional peaks, connected with the presence of N in the InP lattice.

with such intensive energy-transfer rates (with respect to heat propagation), that a quite unstable state originates at each point. The high-temperature gradient between 60 and 100 nm can contribute towards the diffusion of Zn atoms, facilitating their reaction with ion-induced In vacancies. According to TRIM95 modeling, the maximum of these vacancies occurs at depth of about 50–70 nm. Correspondingly, at a power density of 6.5 MW/cm^2 one can find in Fig. 3 a large Zn-concentration plateau of about 9×10^{18} cm^{-3}, extending from 30 to about 100 nm. The overlapping suggests, that the observed behavior of the impurity and the damage can be attributed to the above-mentioned mechanism. In the author's opinion, the appearance of plateau in zinc distribution suggests the existence of critical conditions of the laser irradiation, which favor the recombination of Zn interstitials with In vacancies. Additional experiments to clarify this hypothesis are under way.

D. Micro-Raman spectroscopy

The effect of processing by LPPLA at different nitrogen pressures is studied also by comparing the corresponding Raman spectra. As a reference, Fig. 6 illustrates the spectrum of the virgin InP sample: one can see that the ratio r between the intensities of the transverse (TO) and of longitudinal (LO) optical phonon bands is rather small $[I(\mathrm{TO})/I(\mathrm{LO})\approx0.09]$. This is connected with the fact that TO scattering is forbidden in the backscattering geometry.[31]

In the case of ion implanted sample the spectrum is very similar to the virgin one (see the peak position at 350.5 cm^{-1} and the linewidth of the TO), with only a slight increase of r ($\approx$10%) detected. This is ascribed to partial relaxation of scattering selection rules due to the implantation-induced structural disorder.[32]

Raman spectra change considerably for all samples treated by LPPLA. While the linewidths of the LO band do not change significantly, its peak positions are strongly red-shifted, by 6.8–9.5 cm^{-1}. Simultaneously, a broad asymmetric band appears in the spectra. It is positioned at wave numbers slightly higher than that for the TO band of the virgin InP, but has much higher intensity. These spectral features are characteristic of coupled modes between optical phonons and p-type plasmons. In particular, the red-shift values of the LO peaks are proportional to the p-type carrier concentration.[33,34] The largest red shift (9.5 cm^{-1}) of the LO peak, and therefore the largest activation, corresponds to N_2 pressure of 1.5 atm, in remarkable agreement with the Hall-transport measurements reported in the next section.

Information on the depth characteristics of the implanted region is obtained by comparing the Raman spectra recorded at two different wavelengths, 4579 Å (Fig. 6) and 5145 Å (Fig. 7). The corresponding interaction lengths, defined as sample thickness contributing to 70% of the detected Raman signal, are ~400 and ~900 Å, respectively. The main two bands, in the range of 280–370 cm^{-1}, show similar frequency behavior at both laser wavelengths used. Several new features, not detected in the spectra excited at 4579 Å, appear in the spectra of the annealed samples shown in Fig. 7: a broad band centered at about 420 cm^{-1} and a new peak at

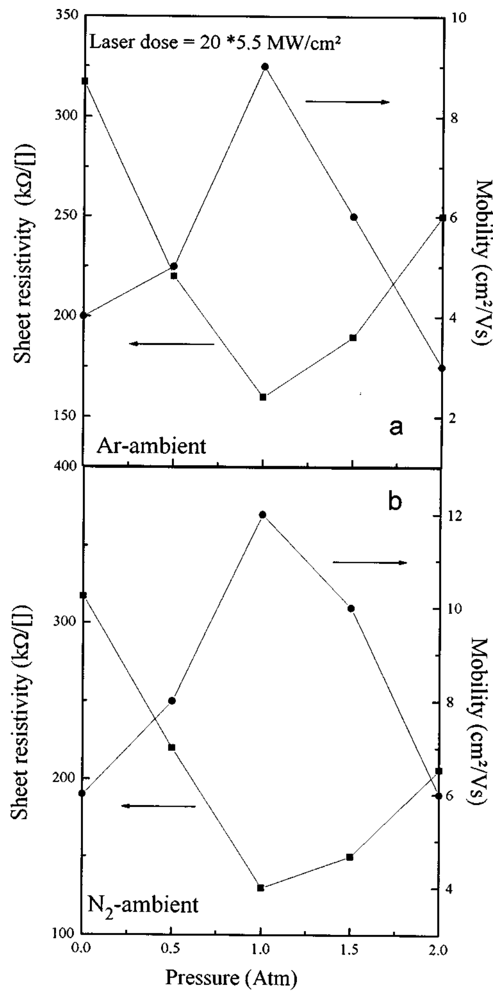

FIG. 8. Sheet resistivity and hole mobility of Zn-implanted GaAs sample treated by LPPLA ($D=20\times 6.5$ MW/cm^2) in Ar (a) and in N_2 (b) ambient correspondingly.

272 cm^{-1} in the spectra of the samples annealed in N_2 atmosphere. The assignment of the features is unclear. It is certain however that it originates from region deeper than 400 Å, in the annealed samples only. The peak at 272 cm^{-1} can be ascribed, by means of computation, to local vibrational modes from Zn substitutional sites. This band appears only in samples annealed under N_2 atmosphere its intensity depending on the N_2 pressure. This fact suggests that the presence of nitrogen atoms favors the implanted Zn^+ atoms to react with ion-induced In vacancies so becoming substitutional in the In sublattice. As a consequence it can be thought that the observed peak has been caused by nitrogen atoms adsorbed at the surface and diffused into the bulk.

E. Electrical measurements

In this section, we summarize the data on the electrical parameters of GaAs and InP samples, processed by laser annealing in a controlled Ar or N_2 atmosphere. The results of the electrical measurements of Zn-implanted GaAs wafers, treated with 20×5.5 MW/cm^2 pulses in Ar atmosphere, are shown in Fig. 8(a). The sheet resistivity and the mobility are given as function of the pressure. It appears that treatment in about 1 atm argon pressure provides best electrical performance. In this conditions ρ_{sheet} has a minimum of about 160 kΩ/□; compared with the value obtained for GaAs annealed in air [450 kΩ/□ (Ref. 35)], it proves the positive effect of the lack of surface oxides on the electrical properties.

With further increase of the argon pressure in the annealing chamber the sheet resistivity rises up and the mobility falls down. In the authors' opinion, this is due to heavy adsorption and diffusion of Ar atoms into the GaAs lattice, where they become interstitial point defects and deteriorate the electrical efficiency. Similar behavior was observed when the gas inlet in the annealing-chamber was changed to nitrogen [Fig. 8(b)]. The sheet resistivity has a minimum of 120 kΩ/□ and the mobility slightly improves with respect to the case of Ar atmosphere, driving the activation rate up by nearly 15%.

The electrical measurements of InP samples processed by LPPLA in Ar or N_2 atmosphere are illustrated in Figs. 9 and 10, respectively. The sheet resistivity [Fig. 9(a)] and the hole mobility [Fig. 9(b)] for samples treated with different irradiation power densities (20×6 MW/cm^2, 20×6.5 MW/cm^2, and 20×7 MW/cm^2) are plotted against the Ar pressure in the annealing chamber. In this case the hole mobility maximum (23 cm^2/V s) and the sheet resistivity minimum (18 kΩ/□) occur at Ar pressure of 1.5 atm and irradiation power density of 6.5 MW/cm^2. The best activation rate obtained is about 18%. At argon pressures exceeding 1.5 atm, some degradation of the electrical properties is observed. It is probably connected with the adsorption and diffusion of Ar atoms as interstitial point defects, mentioned earlier for the GaAs case.

More encouraging results have been obtained for Zn^+-implanted InP samples, annealed by laser in N_2 atmosphere (Fig. 10). The dependencies of ρ_{sheet} and μ for wafers annealed at different laser power densities are given as functions of the N_2 pressure in the annealing chamber. The curves demonstrate mainly three features.

(a) The conductivity and mobility values measured for InP samples, which have been annealed in vacuum, are really not satisfactory. The critical temperature (defined as temperature above which the compound stoichiometry alters), depending mainly on the partial pressure of the phosphorus in the vapor phase, decreases in vacuum. As a consequence, an irradiation power density of 6.5 MW/cm^2 does not guarantee the compound integrity anymore.

(b) The maximum values of the conductivity and the mobility occur exactly at the same experimental conditions (laser power density and pressure) as those found earlier in InP sample annealed in Ar atmosphere.

(c) The maximum of the hole mobility obtained in our experiments is about 70 cm^2/V s. Such a high value is normally coupled with high resistivity, and therefore low-carrier concentration. On the contrary, the minimum of the sheet resistivity (of about 1 kΩ/□) is combined in our case with high-carrier concentration ($p_{\square}=8\times 10^{13}$ cm^{-2}) and electrical activation of nearly 80%.[36,37]

The above reported changes of the electrical properties of InP with nitrogen pressure are connected evidently with the adsorption and diffusion processes taking place during the laser irradiation. Similar to argon, the adsorbed N atoms can diffuse in the host matrix; due to the chemical affinity to P they can be trapped in P vacancies and become substitutional

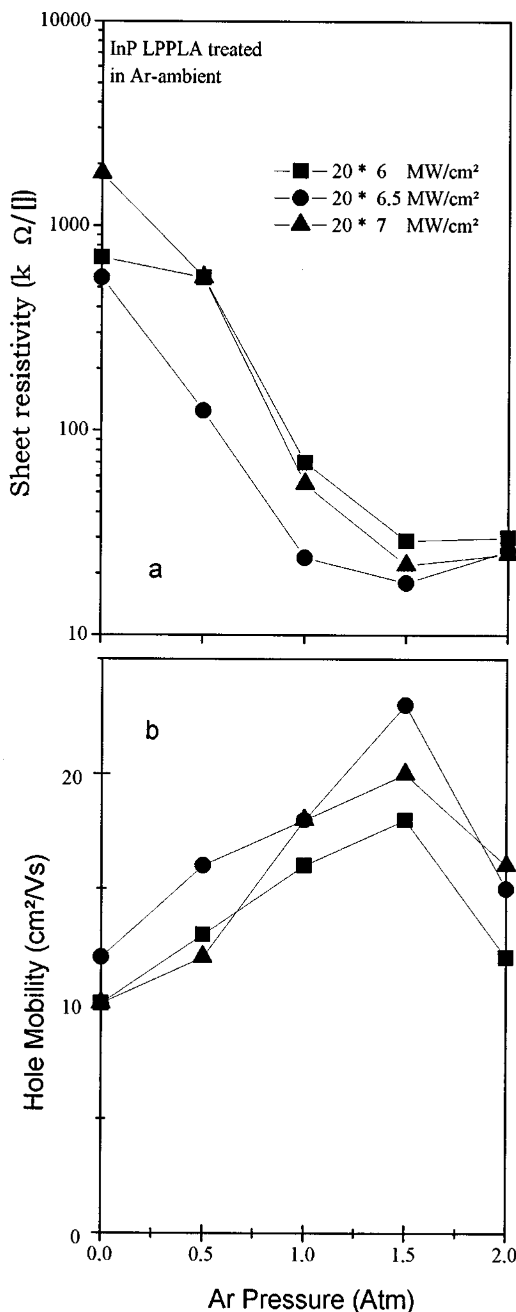

FIG. 9. Sheet resistivity (a) and hole mobility (b) as a function of Ar pressure in the annealing chamber. LPPLA treatment of Zn-implanted InP with 20 pulses at different power densities.

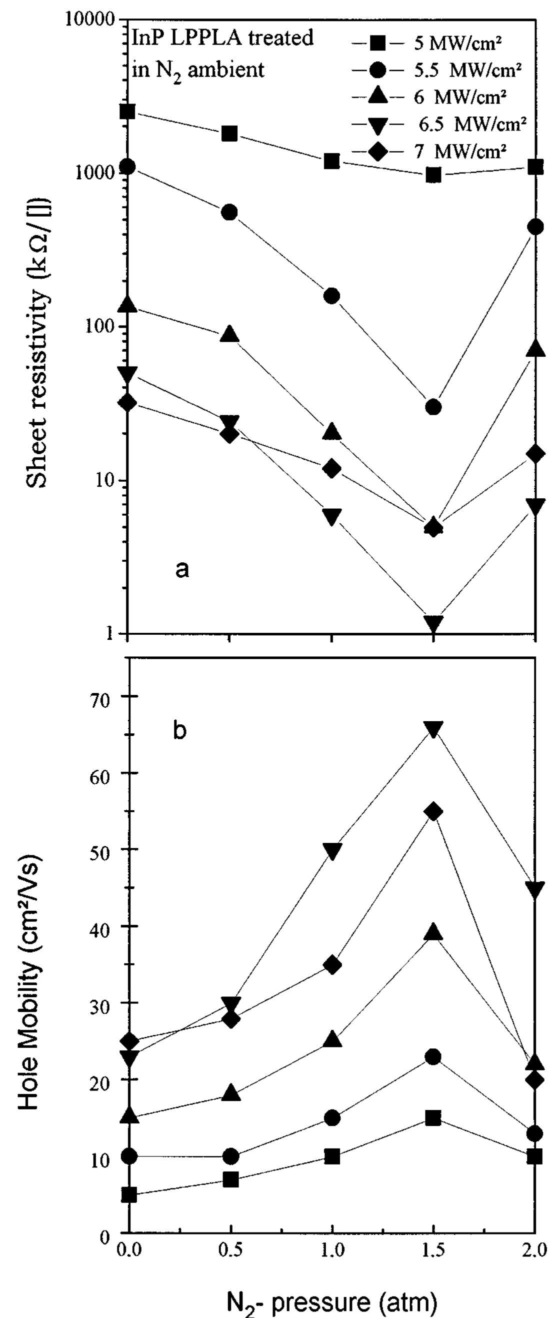

FIG. 10. Sheet resistivity (a) and hole mobility (b) of Zn-implanted InP as a function of the pressure of N_2 ambient in the annealing chamber LPPLA treatment with 20 pulses of different power densities.

in the P sublattice. Thus, besides preventing surface-oxide formation, the role of N_2 atmosphere is to contribute to the saturation of P vacancies. The implanted Zn^+ ions, freed by the laser action as described above, will react favorably with the ion-induced In vacancies and become substitutional in the In sublattice, acting as electrically activated extrinsic carriers.[38] The obtained maxima of σ_{sheet} and μ in these experimental conditions (6.5 MW/cm^2 and 1.5-atm N_2 pressure) indicate that some equilibrium between P losses and N adsorption is achieved, resulting in saturation of P vacancies; as a consequence, the majority of Zn implants are forced to occupy In sites. With further increase of the nitrogen pressure, the electrical performance is worsened since some of the excess adsorbed N atoms cannot find vacant P sites and remain interstitials. The latter act as simple contaminating impurities and degrade the electrical parameters such as μ and ρ_{sheet} values (see Fig. 10).

Similar assumption was published recently in a discussion of Zn^+ and As^+ coimplantation in InP:[39] the authors of this paper conclude that As^+implantation in InP preimplanted with Zn^+ leads to stoichiometric alteration of the implanted layer. Namely, the increase of the concentration of In vacancies facilitates the redistribution and incorporation of Zn impurities in the cationic sublattice and therefore the annealing of the radiation defects and the activation of the acceptor Zn

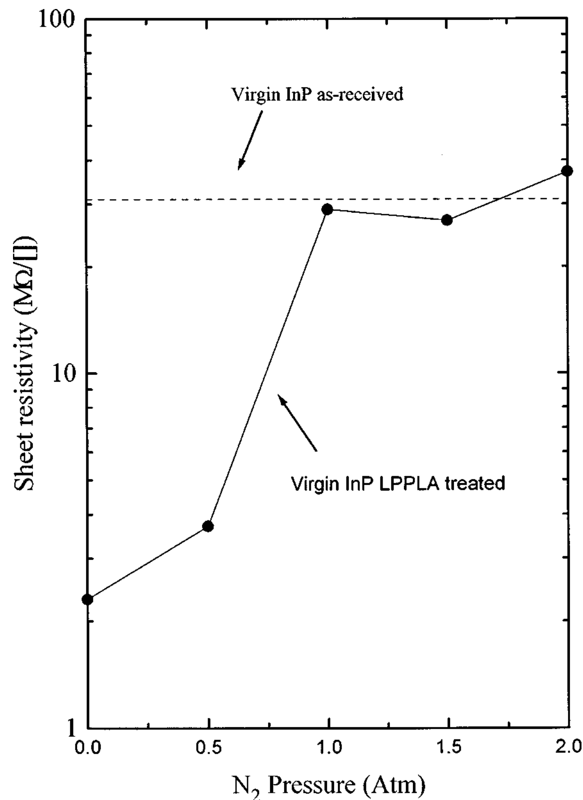

FIG. 11. Sheet resistivity of virgin (dashed line) and virgin +LPPLA treated (by 20 pulses of 6.5 MW/cm^2) InP as a function of the N_2 pressure in the annealing chamber.

impurities. This interpretation supports the mechanism of solid-state recrystallization and the electrical carrier activation by LPPLA suggested above.

To verify the possibility that the contribution of N atoms is related to the doping of InP, we performed the following experiments. Virgin (unimplanted) InP samples were exposed to 20×6.5 MW/cm^2 laser pulse irradiation at different pressures of the nitrogen ambient in the annealing chamber. After the LPPLA treatment the sheet resistivity of the specimens as function of the pressure was measured and compared with that of the untreated virgin sample (Fig. 11). With increasing the N_2 pressure the value of ρ_{sheet} rises till the reference ρ_{sheet} value of the nontreated sample is achieved. Small values of sheet resistivity at low-N_2 pressure can be justified assuming hopping conduction associated with substantial P losses in the highly damaged surface layer. As N_2 pressure increases, ρ_{sheet} increases too, up to the value of the untreated sample it supports the assumption that the nitrogen atoms affect the electrical properties without dope the InP samples.

IV. CONCLUSIONS

The role of LPPLA in the lattice recovery and the electrical activation of III-V semiconductors is studied using several complementary techniques. The HRTEM patterns demonstrate on atomic level the efficiency of the laser processing in restoring the crystal structure of compound semiconductors damaged by ion implantation. RBS spectra also indicate excellent lattice reordering. In some particular annealing conditions the damage yield in the spectra is even lower than that obtained from virgin samples. SIMS analysis of the annealed samples proves the diffusion of Zn atoms toward the surface. In the best annealing conditions a flat distribution of the implanted zinc has been obtained, within a layer 70–80 nm thick, centered at about 50 nm below the surface. This plateau is assumed to be connected with the presence of substitutional zinc in the In sublattice. The micro-Raman spectroscopy confirms this interpretation by the appearance of a large band at wave numbers slightly larger than those of the TO phonons. This band can be ascribed to coupled modes between optical phonons and *p*-type plasmons. Furthermore, some red shift proportional to the *p*-type carrier concentration appears in the annealed samples. The maximum of this shift occurs at the best annealing conditions (in terms of electrical properties). Finally, some spectral features appear (e.g., peak centered at wave number of 272 cm^{-1}) depending on the N pressure. These spectral features change as the excitation laser wavelength is varied from 4159 to 5145 Å. Since the detected signals come from a layer of thickness 40 and 90 nm, respectively and depend on the nitrogen pressure in the annealing chamber, one may argue that these spectral features can be related to local vibrational modes from Zn substitutional atoms in a layer about 50 nm thick, of the order of 40 nm below the sample surface. This result agrees well with the flat Zn concentration at these depths, as observed by SIMS. The presence of N atoms in this layer stimulates the substitutional positioning of Zn atoms in the In sublattice. The electrical measurements for InP samples irradiated in nitrogen atmosphere are very conclusive. It is worth noticing that we were able to achieve an electrical activation rate of about 80% for carriers, originated from acceptor-type impurities. This value is higher than those obtained by using conventional techniques even for donor-type impurities. Compared to the annealing results in inert atmosphere, we can conclude that the observed rate is mainly due to the chemical affinity between nitrogen and phosphorous. For GaAs, the annealing in N_2 atmosphere still gives results better than those obtained in Ar atmosphere. The improvement effect is however less than in InP, which we can relate to the fact that the chemical affinity is not so strong as in the InP case.

The fundamental role played by the nitrogen atoms in the formation of electrically active impurities is therefore evidenced: during the LPPLA processing the N atoms diffuse into the material and fill the P sites in the lattice. As a consequence Zn atoms can react with In vacancies and occupy substitutional states as electrically activated *p*-type carriers. Within this layer the nitrogen atoms change the composition substantially and the material can be considered as azotized compound semiconductor.

ACKNOWLEDGMENT

The present work was partially supported by the Bulgarian Ministry of Education and Science through the Φ 818 and Φ 822 projects.

[1] J. P. Donnelly and C. E. Hurwitz, Appl. Phys. Lett. **31**, 418 (1977).
[2] D. E. Davies, J. P. Lorenzo, and T. G. Ryan, Solid-State Electron. **21**, 981 (1978).
[3] J. J. Berenz, F. G. Frank, and T. L. Hierl, Electron. Lett. **14**, 683 (1978).
[4] J. P. Donnelly and C. E. Hurwitz, Solid-State Electron. **21**, 475 (1978).
[5] W. T. Devlin, K. T. Ip, D. P. Leta, L. F. Eastman, and G. H. Morrison, in *Gallium Arsenide and Related Compounds*, edited by C. M. Wolfe, IOP Conf. Proc. No. 45 (Institute of Physics, Bristol, 1978), p. 510.
[6] J. P. Donnelly and C. A. Armiento, Appl. Phys. Lett. **34**, 96 (1979).
[7] C. A. Armiento, J. P. Donnelly, and J. P. Lorenzo, Appl. Phys. Lett. **34**, 239 (1979).
[8] E. Eirug Davies, W. D. Potter, and J. P. Lorenzo, J. Electrochem. Soc. **125**, 845 (1978).
[9] M. Yamaguchi, T. Takamoto, and M. Ohmori, J. Appl. Phys. **81**, 1116 (1997).
[10] C. J. Keavney and M. B. Spitzer, Appl. Phys. Lett. **52**, 1439 (1988).
[11] T. Inada, S. Taka, and Y. Yamamoto, Nucl. Instrum. Methods **182/183**, 641 (1981).
[12] R. F. Davies, Proc. IEEE **79**, 701 (1991).
[13] S. Strite and H. Morkoc, J. Vac. Sci. Technol. B **10**, 343 (1994).
[14] G. Mohs, B. Fluegel, H. Geissen, H. Tajalli, N. Peyghambarian, P. C. Cjiu, B. S. Phillips, and M. Osinski, Appl. Phys. Lett. **67**, 1515 (1995).
[15] S. Nakamura, T. Mukai, and X. Senoh, Appl. Phys. Lett. **64**, 1687 (1994).
[16] W. G. Bi and C. W. Tu, J. Appl. Phys. **80**, 1934 (1996).
[17] P. Soukiassian, T. Kendelwitz, H. I. Starnberg, M. H. Bakshi, and Z. Hurych, Europhys. Lett. **12**, 87 (1990).
[18] K. Wang, Appl. Phys. Lett. **25**, 2127 (1987).
[19] K. V. Vaidyanathan, C. L. Anderson, H. L. Dunlap, and D. E. Holmes, Nucl. Instrum. Methods **182/183**, 631 (1981).
[20] J. D. Oberstar, B. G. Streetman, J. E. Baker, and P. Williams, J. Electrochem. Soc. **129**, 1312 (1982).
[21] R. Ahuja, S. Auluck, O. Eriksson, J. M. Mills, and B. Johansson, Solid State Commun. **104**, 249 (1997).
[22] R. J. Walters, S. R. Messenger, H. L. Cotal, G. P. Summers, and E. A. Burke, Solid-State Electron. **39**, 797 (1997).
[23] B. Molnar, G. Kelner, G. L. Ramseyer, G. H. Morrison, and S. C. Shatos, in *Fly Ash and Coal Conversion By-Products: Characterization, Utilization, and Disposal*, edited by G. J. McCarthy and R. J. Lauf, MRS Symposia Proceedings No. 45 (Materials Research Society, Pittsburgh, 1985), p. 329.
[24] M. V. Rao and R. K. Nadella, J. Appl. Phys. **67**, 1761 (1990).
[25] U. Konig, J. Hilgarth, and H. H. Tiemann, J. Electron. Mater. **14**, 311 (1985).
[26] G. Vitali, L. Palumbo, M. Rossi, G. Zollo, C. Pizzuto, L. DiGaspare, and F. Evangelisti, Phys. Rev. B **53**, 4757 (1996).
[27] G. Vitali, G. Zollo, C. Pizzuto, M. Rossi, D. Manno, and M. Kalitzova, Appl. Phys. Lett. **26**, 4072 (1996).
[28] J. Borgoun and M. Lannoo, *Point Defects in Semiconductors II: Experimental Aspects* (Springer-Verlag, Berlin, 1983).
[29] G. Vitali, Jpn. J. Appl. Phys., Part 1 **31**, 2049 (1992).
[30] Y. Siegal, E. N. Glazer, L. Huang, and E. Mazur, Annu. Rev. Mater. Sci. **25**, 223 (1995).
[31] G. Zollo, L. Palumbo, M. Rossi, and G. Vitali, Appl. Phys. A: Solids Surf. **56**, 409 (1993).
[32] E. Bedel, G. Landa, R. Carles, J. B. Renucci, J. M. Roquais, and P. N. Favennec, J. Appl. Phys. **60**, 1980 (1986).
[33] D. Olego and M. Cardona, Solid State Commun. **32**, 375 (1979).
[34] D. Olego and M. Cardona, Phys. Rev. B **24**, 7217 (1981).
[35] G. Vitali, C. Pizzuto, M. Rossi, G. Zollo, D. Karpuzov, and M. Kalitzova, Jpn. J. Appl. Phys., Part 1 **33**, 5 (1994).
[36] C. Pizzuto, G. Zollo, G. Vitali, D. Karpuzov, and M. Kalitzova, J. Appl. Phys. **82**, 3447 (1997).
[37] G. Vitali, C. Pizzuto, and G. Zollo, Solid State Commun. **106**, 421 (1998).
[38] C. Pizzuto and G. Vitali, Italy Patent, No. RM A000064 (pending).
[39] I. M. Tiginyanu, I. V. Kravetsky, V. V. Ursaki, G. Marowsky, and H. L. Hartnagel, Phys. Status Solidi A **162**, K9 (1997).